

# Multi-Responsive Biodegradable Cationic Nanogels for Highly Efficient Treatment of Tumors

Xin Li, Haitao Sun, Helin Li, Chaolei Hu, Yu Luo,\* Xiangyang Shi,\* and Andrij Pich\*

The facile preparation, modular design, and multi-responsiveness are extremely critical for developing pervasive nanoplateforms to meet heterogeneous applications. Here, cationic nanogels (NGs) are modularly engineered with tunable responsiveness, versatility, and biodegradation. Cationic PVCL-based NGs with core/shell structure are fabricated by facile one-step synthesis. The formed PVCL-NH<sub>2</sub> NGs exhibit uniform size, thermal/pH dual-responsive behaviors, and redox-triggered degradation. Moreover, the NGs can be employed to modify or/and load with various functional agents to construct multipurpose nanoplateforms in a modular manner. Notably, the novel hybrid structure with copper sulfide (CuS) NPs loaded in the NGs shell is prepared, which leads to higher photothermal conversion efficiency (31.1%) than other CuS randomly loaded NGs reported. By personalized tailoring, these functionalized NGs display fluorescent property,  $r_1$  relaxivity, strong near-infrared (NIR) absorption, good biocompatibility, and targeting specificity. The superior photothermal effect of hybrid NGs (CuS@NGs-LA) is presented under NIR II over NIR I. Importantly, hybrid NGs encapsulated doxorubicin (CuS@NGs-LA/DOX) show endogenous pH/redox and exogenous NIR multi-triggered drug release for efficient photothermal-chemotherapy, which can completely eliminate advanced tumors and effectively inhibit recurrence. Overall, the pervasive nanoplateforms based on intelligent cationic NGs with tunable responsiveness, versatility, and biodegradation are developed by engineered modular strategy for precision medicine applications.


## 1. Introduction

In recent years, a series of multifunctional nanoplateforms have been developed for precision medicine to improve the diagnosis accuracy and treatment efficiency of the diseases.<sup>[1]</sup> However, an extreme challenge within the field is the requirement for construction of versatile nanoplateforms that need to be tailored to individual patients.<sup>[2]</sup> Currently, a common approach can be utilized to design highly tailored nanoplateforms that target specific lesion tissues via recognition of overexpressed cellular markers. What is more, the nanoplateforms with stimuli-responsiveness as nanocarriers are able to effectively deliver therapeutic agents to the targeted region and release controllably them by the endogenous or exogenous stimulation, and thus achieve precision medicine applications.<sup>[3]</sup> Normally, the nanoplateforms integrate multiple therapeutics that can act synergistically to kill cancer cells.<sup>[4]</sup> Compared with all existing cancer treatment methods, photothermal therapy (PTT), especially in the near-infrared II window (NIR II), is introduced

X. Li, H. Li, C. Hu, Prof. A. Pich  
DWI-Leibniz-Institute for Interactive Materials e.V.  
Forckenbeckstr. 50, 52056 Aachen, Germany  
E-mail: pich@dwil.rwth-aachen.de

X. Li, H. Li, C. Hu, Prof. A. Pich  
Institute for Technical and Macromolecular Chemistry  
RWTH Aachen University  
Worringerweg 2, 52074 Aachen, Germany

H. Sun  
Department of Interventional Radiology  
Zhongshan Hospital  
Shanghai Institute of Medical Imaging  
Fudan University  
180 Fenglin Road, Shanghai 200032, P. R. China

 The ORCID identification number(s) for the author(s) of this article can be found under <https://doi.org/10.1002/adfm.202100227>.

© 2021 The Authors. Advanced Functional Materials published by Wiley-VCH GmbH. This is an open access article under the terms of the Creative Commons Attribution License, which permits use, distribution and reproduction in any medium, provided the original work is properly cited.

DOI: 10.1002/adfm.202100227

Dr. Y. Luo  
School of Chemical Science and Engineering  
Tongji University  
1239 Siping Road, Shanghai 200092, P. R. China  
E-mail: yuluo@tongji.edu.cn

Prof. X. Shi  
College of Chemistry  
Chemical Engineering and Biotechnology  
Donghua University  
2999 North Renmin Road, Shanghai 201620, P. R. China  
E-mail: xshi@dhu.edu.cn

Prof. X. Shi  
CQM-Centro de Química da Madeira  
Campus da Penteada  
Universidade da Madeira  
Funchal 9000-390, Portugal

Prof. A. Pich  
Aachen Maastricht Institute for Biobased Materials  
Maastricht University  
Geleen 6167 RD, Netherlands

to effectively eliminate solid tumors with large area via hyperthermia ablation.<sup>[5]</sup> Likewise, the chemotherapy (CMT) emerges to clean up the infiltrating and metastatic cancer cells, and thus inhibit tumor recurrence.<sup>[6]</sup> Remarkably, the combined PTT and CMT can significantly improve the outcomes of synergistic therapy for clinical use.<sup>[7]</sup>

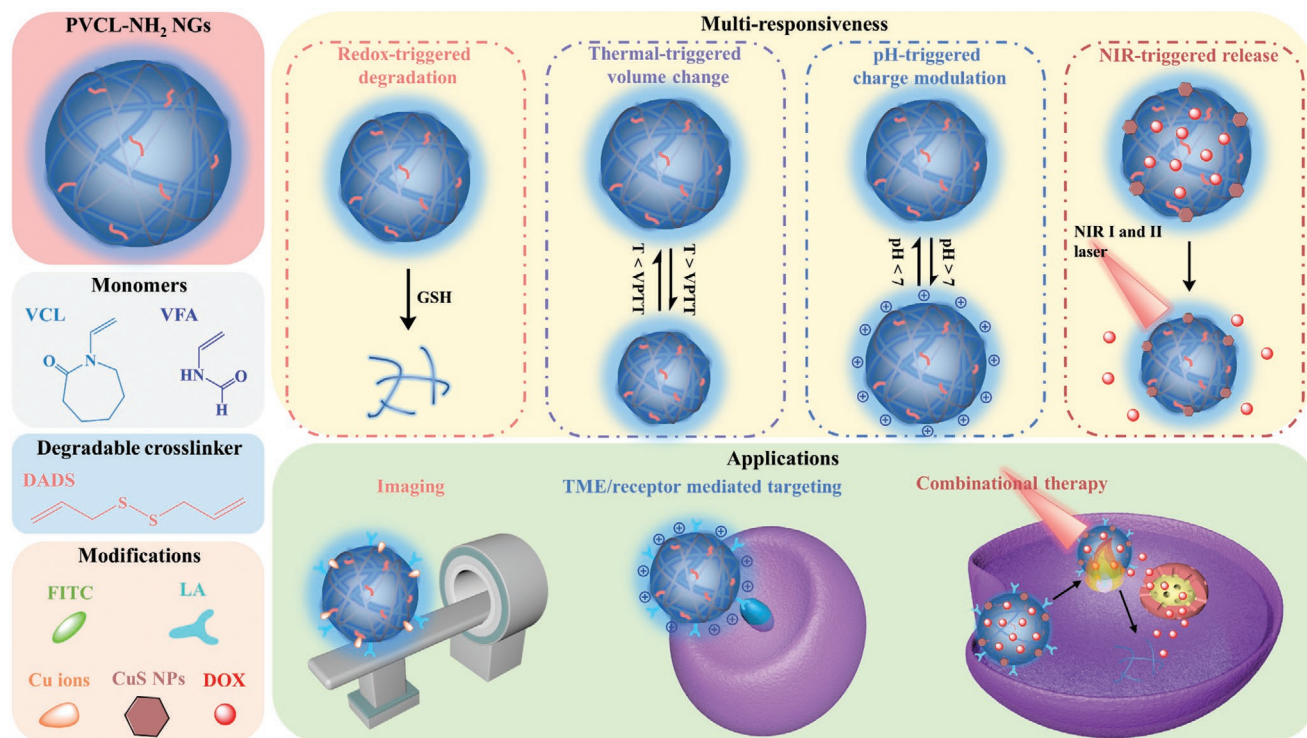
For individual patient or pathology, the precise and tailored treatment is necessitated due to the marked variability between patients. In the previous studies,<sup>[8]</sup> precision medicines have focused on highly specified nanoplateforms that efficiently target and kill single tumor population. Nowadays, the major hurdles need to overcome by engineer highly the tunable nanoplateforms technologies integrating multiple therapeutic modalities. In this work, the engineered modular strategy is performed to address the challenge and serve as a useful tool for the next generation of cancer theranostic protocol.

Nanogels (NGs), a class of 3D cross-linked polymer colloids, have attracted great attention in the biomedical applications,<sup>[9]</sup> due to the deformable shape, controllable size, good biocompatibility, and excellent loading capacity. Among them, the NGs with amino groups are of considerable interest for easy post-modification with a diversity of functional molecules, including, but not limit to, proteins, chelations, zwitterions, fluorescent molecules, and targeted agents, via the amine chemistry.<sup>[10]</sup> The post-modification of NGs offers access to complex their architectures and augment their applications in various fields.<sup>[11]</sup> Moreover, the amino groups display cationic nature, which can be used for loading drug or compressing gene,<sup>[12]</sup> elevating tissue permeation and cellular uptake via active transportation.<sup>[13]</sup> In very recent work, Chan et al.<sup>[14]</sup> evidenced that active transportation is the dominant mechanism transport

most of nanoparticles (NPs) into solid tumors but not passive diffusion. Additionally, the stimuli-responsive cationic polymers were developed as nanocarriers to deliver cargoes deeply into the tumor by active transportation, and exerted potent activity for tumor treatment.<sup>[15]</sup> Therefore, the engineered construction of cationic NGs is urgently needed for effective biomedical applications.

Normally, the cationic NGs with abundant amino groups can be synthesized by two ways: 1) The crosslinking of the primary amine-based polymers using miniemulsion method,<sup>[10c]</sup> and 2) the polymerization of primary amine functional monomers with hydrochloride protection,<sup>[16]</sup> because of the presence of free primary and secondary amines making the polymerization impossible. However, the former are complex operating procedures, hard-to-purify attributes, low yields, and non-uniform size distribution. For the latter, the protection/deprotection steps in acidic conditions may lead to the hydrolysis of other comonomers during the polymerization. Therefore, the synthesis of cationic NGs with controlled size and high yield based on one-step method is also extremely challenging.

Here, a modular engineered strategy for the preparation of pervasive cationic NGs with tunable responsiveness, versatility, and biodegradation was first developed (**Scheme 1**). The core/shell structured PVCL-based NGs enabling the adjustable content of amino groups were synthesized using a facile one-step method. The formed cationic NGs exhibit thermal/pH/redox multi-responsive behaviors and are employed to modify or/and load with various functional agents (fluorescent dyes, targeting molecules, metal ions, NPs, and drugs) to construct multipurpose nanoplateforms in a modular manner. Notably, the novel hybrid NGs (CuS@NGs-LA) were obtained by loading of copper



**Scheme 1.** Overview of modular nanoplateforms based on cationic NGs for precision theranostic applications.

sulfide (CuS) NPs in the shell of NGs, that may permit to facilitate more full contact with NIR laser, leading to higher photothermal conversion efficiency (PCE, 31.1%) than other PCE of CuS randomly loaded NGs reported in the previous work.<sup>[10b]</sup> These NGs derivatives can be utilized for personalized tailoring, and thus have diversified potential applications in personalized theranostics of fluorescence and magnetic resonance (MR) imaging, controlled drug release in responding to endogenous pH/redox and exogenous NIR, combinational PTT and CMT under safe NIR II irradiation. The superior photothermal effect of CuS@NGs-LA is achieved under NIR II over NIR I due to higher PCE and deeper tissue penetration. Encouragingly, the created hybrid NGs encapsulated doxorubicine (CuS@NGs-LA/DOX) by systemic injection can completely eliminate advanced solid tumors and effectively inhibit recurrence in vivo through the combined therapy.

## 2. Results and Discussion

### 2.1. Synthesis and Characterization of PVCL-NH<sub>2</sub> Nanogels

PVCL-VFA NGs with core/shell morphology were synthesized by the precipitation polymerization. The *N*-vinylformamide (VFA) with 25 mol% amount was added after the initiation of polymerization of *N*-vinylcaprolactam (VCL) to ensure the formation of core/shell structure. Then, the amino groups on the periphery of NGs were generated by the direct hydrolysis of aldehyde (–CHO) groups of VFA under alkaline conditions. The transmission electron microscopy (TEM) images revealed that the core/shell NGs at different hydrolysis times displayed narrow size distribution and uniform diameters (about 80 nm) (Figure 1a). Likewise, the hydrodynamic diameters of these NGs were measured to be 132–163 nm by dynamic light scattering (Figure 1b and Figure S1, Supporting Information), which are bigger than that measured by TEM imaging, due to the swelling state of NGs in the aqueous solution. Our previous work verified that the size of NGs between 100–200 nm is suitable for enhanced tumor accumulation by EPR effect and improved penetration in biomedical applications.<sup>[10b]</sup>

Besides, the conversion from –CHO to –NH<sub>2</sub> groups on the NGs after different hydrolysis times was characterized using <sup>1</sup>H NMR spectroscopy (Figure 1c and Figure S2, Supporting Information). The signal of –CHO at about 8.3 ppm was decreased progressively attributing to the increased hydrolysis time, suggesting the conversion from –CHO to –NH<sub>2</sub> groups increased. By the integration of NMR (Figure 1d), after hydrolysis for 48 h, the –CHO molar contents of NGs decreased from 21.3% to 10.2%, and thus the conversion ratios of aldehyde into amine were elevated to 0.52. FTIR spectra (Figure S3, Supporting Information) indicated that the typical peak at 1520–1600 cm<sup>–1</sup> for PVCL-NH<sub>2</sub> NGs, which could be contributed to the in-plane-bending of N–H bond, originating from the amino groups was significantly enhanced when compared to PVCL-VFA NGs.<sup>[17]</sup> Furthermore, the formed PVCL-NH<sub>2</sub> NGs dispersed in different media did not display any significant change in the hydrodynamic size for at least 5 days (Figure S4, Supporting Information), suggesting their excellent long-term colloidal stability.

More importantly, compared with the emulsion method for the preparation of NGs with amino groups, the designed approach of facile one-step synthesis is capable of preparing core/shell amino-terminal NGs with high yields, uniform morphology, low PDI, uniform and proper size.

### 2.2. pH/Thermal-Responsive Behavior and Redox-Triggered Degradation

The formed PVCL-NH<sub>2</sub> NGs exhibiting pH/thermal dual-mode responsive behavior were investigated at different temperatures (5–50 °C) and pHs (3–10), respectively. The PVCL-NH<sub>2</sub> NGs showed the volume phase transition temperature (VPTT) of 32.4 °C (Figure 2a). With the temperature increase, the hydrodynamic diameters of PVCL-NH<sub>2</sub> NGs were reduced to about 120 nm at temperature above VPTT. Moreover, the pH-triggered charge modulation of PVCL-NH<sub>2</sub> NGs was observed due to their abundant amino groups (Figure 2b). The PVCL-VFA NGs showed slight positive charge since the cationic initiator was used in the reaction. As a comparison, the obviously higher positive charge was observed in PVCL-NH<sub>2</sub> NGs at pH 7, suggesting more amino groups were successfully formed after hydrolysis. By virtue of the amino groups that can acquire H<sup>+</sup> to form –NH<sub>3</sub><sup>+</sup> in the acidic environment, the PVCL-NH<sub>2</sub> NGs emerged the increased electrophoretic mobility from 0.051 to 1.72 in the pH ranges (10 to 3). The pH-responsive cationization of NGs is beneficial to elevate their affinity with cell membranes under acidic tumor microenvironment (TME), leading to the enhanced cellular internalization.

The biodegradability of NGs is a crucial feature for biomedical applications. The redox-triggered degradation of PVCL-NH<sub>2</sub> NGs in the simulated redox TME (10 mM GSH, 37 °C) was investigated by TEM images (Figure 2d). The NGs were progressively degraded via disulfide bonds cleavage of crosslinkers under GSH environment. Furthermore, the quantitative degradation of NGs with or without GSH was determined by mass loss (Figure 2c). During the first 4 h, the weight of NGs decreased rapidly under GSH environment and the mass loss reached around 48%. After 20 h, the mass loss of NGs was about 93% and then achieved equilibrium. These results suggest that under redox TME, the NGs can be degraded completely into small fragments which would be rapidly metabolized from the body to reduce toxicity and risk of long-term retention.

### 2.3. Modification of Bioactive Components

For ideal nanoplatfoms, multifunctional modification is very important for aplenty their architectures and broadening their applications. The amino-terminal NGs can be allowed to modify a diversity of functional molecules via facile amine chemistry to construct versatile nanoplatfoms according to the desired properties. First, fluorescent molecule (fluorescein isothiocyanate, FI), as the representative of the molecules containing isothiocyanate groups, was covalently attached to NGs (Figure 3a). Using UV–vis spectra (Figure 3b and Figure S5, Supporting Information) and fluorescence imaging (Figure 3c),



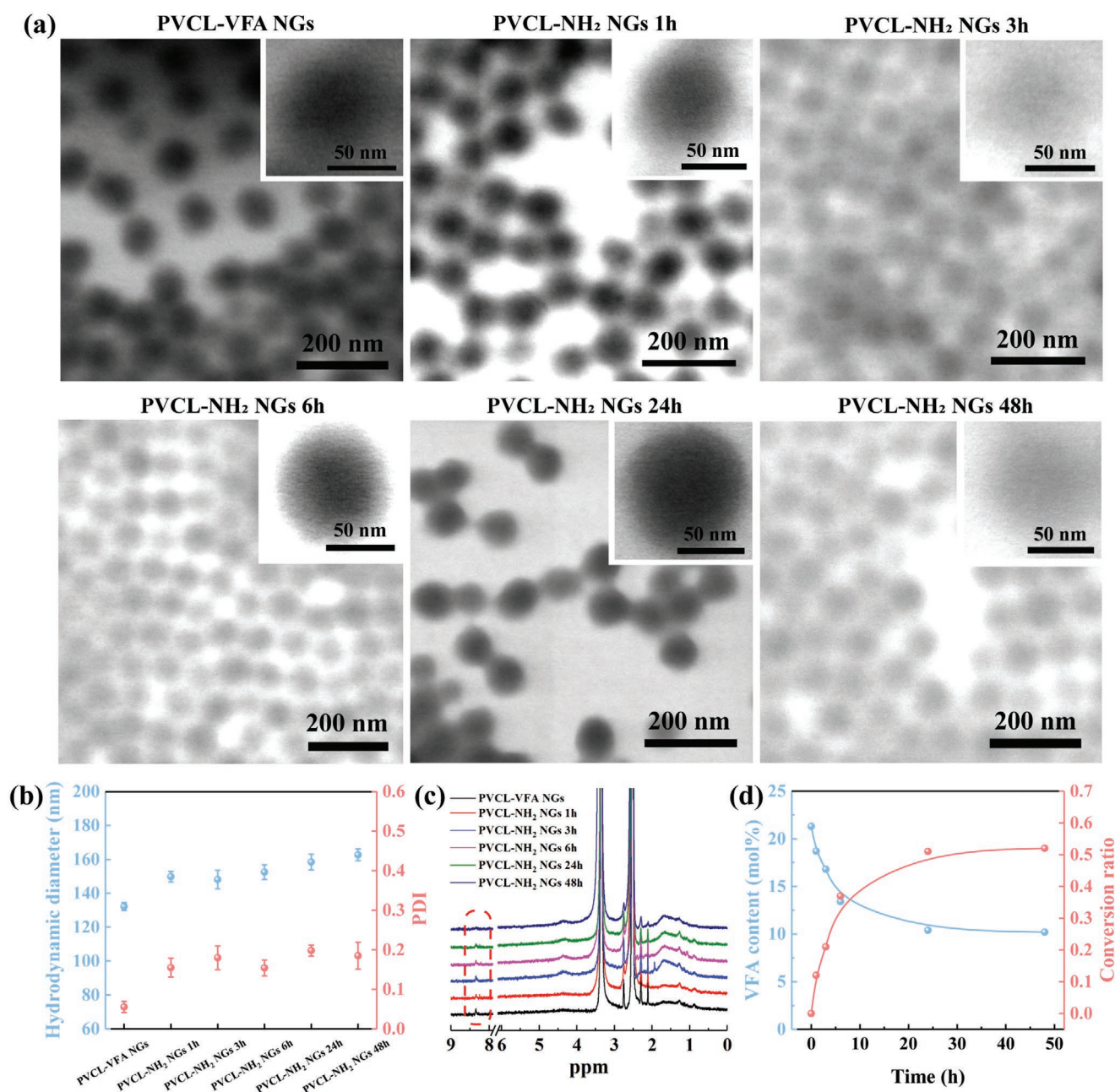


**Figure 1.** a) TEM images, b) hydrodynamic diameters and PDI, c) <sup>1</sup>H NMR spectra (in DMSO-*d*<sub>6</sub>), d) VFA molar contents and amino conversion ratios of PVCL-VFA NGs and PVCL-NH<sub>2</sub> NGs with different hydrolysis times.

we observed that the NGs-FI were successfully prepared and the FI amounts on NGs-FI increased with FI/–NH<sub>2</sub> ratios, and then the FI amounts were calculated to be about 0.61 mg·mg<sup>−1</sup> when the ratio reached 1:1 (Figure 3b). The NGs-FI is expected as a fluorescent nanoplatform for the potential application of cell imaging or tracing. Second, the targeted molecule (lactobionic acid, LA), as a class of functional molecules containing carboxyl groups, was able to react with NGs by EDC chemistry (Figure 3a). Through the integration of NMR (Figure 3d), the LA molar contents of the prepared NGs-LA increased from 1.3% to 9.7% with the ratios of LA/–NH<sub>2</sub>. The conjugation

of LA on the NGs can endow them with excellent targeting capacity and good biocompatibility. Besides, based on the previous reports,<sup>[8c,18]</sup> the amino and carbonyl groups are capable of binding and stabilizing some metal ions, such as, Fe(III), Cu(II), or Au (III). To reserve part of amino groups for subsequent modification, the NGs-LA prepared at the LA/–NH<sub>2</sub> ratio of 1:2 were employed to bind Cu(II) due to their carbonyl and residual amino groups (Figure 3a). By the ICP-OES measurement, as the addition of Cu(II) increases, the Cu(II)@NGs-LA exhibited a maximum binding amount of Cu (II) as high as 59 μg mg<sup>−1</sup> of Cu(II)/NGs (Figure 3e). According to our

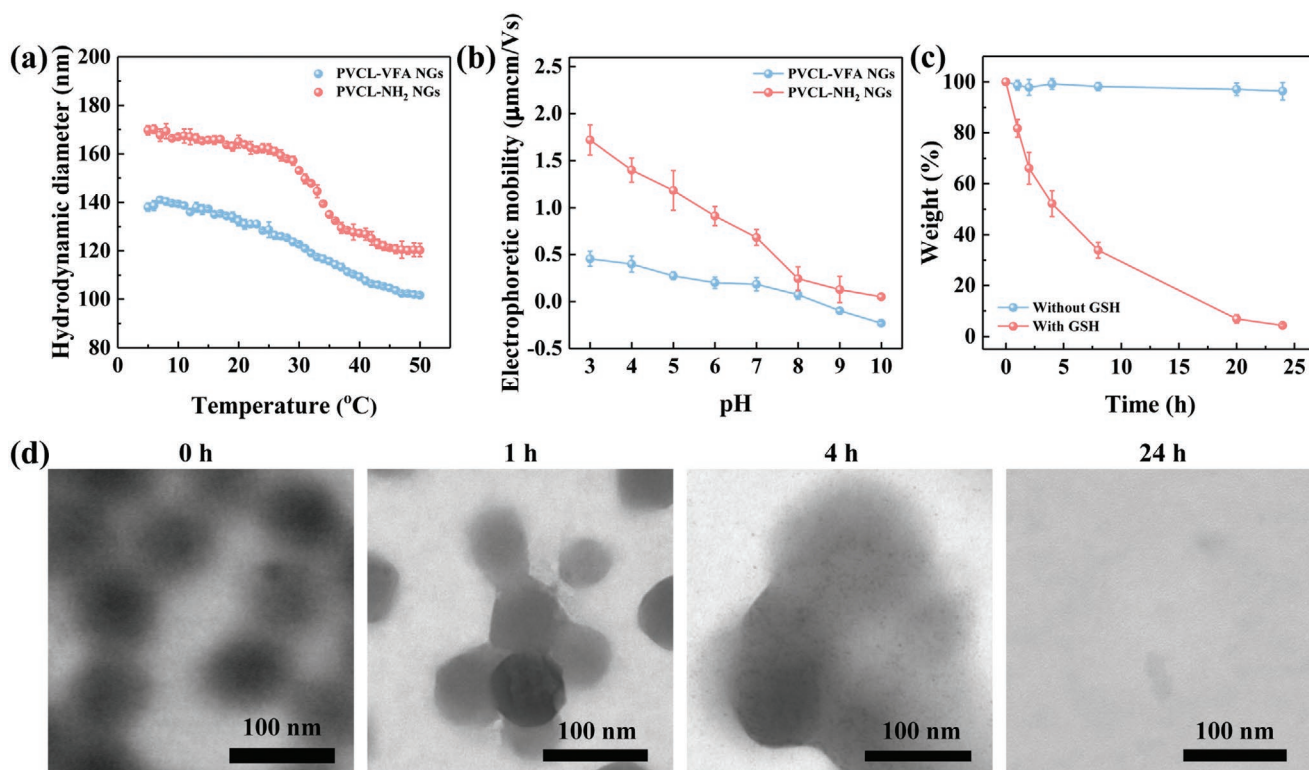


**Figure 2.** a) Hydrodynamic diameter and b) electrophoretic mobility change of the PVCL-VFA NGs and final PVCL-NH<sub>2</sub> NGs at different temperatures and pHs, respectively. c) Weight loss and d) TEM images of PVCL-NH<sub>2</sub> NGs in the presence of GSH (10 mM) at 37 °C for different times.

previous work,<sup>[19]</sup> the Cu(II) chelated nanoplateforms can be used as theranostic agents for MR imaging and free-drug CMT of cancers. Hereby,  $T_1$  relaxation rate of Cu(II)@NGs-LA and CuCl<sub>2</sub> was determined to evaluate their capacity in  $T_1$  MR imaging (Figure 3f). The  $r_1$  relaxivity of Cu(II)@NGs-LA was calculated to be 0.826 mM<sup>-1</sup> s<sup>-1</sup>, higher than that of pure Cu (II) salt (0.719 mM<sup>-1</sup> s<sup>-1</sup>). The relatively higher  $r_1$  relaxivity may be due to the increased hydrodynamic size of Cu(II)@NGs-LA that renders Cu(II) to have the extended rotational correlation time, in agreement with the work regarding Gd(III)-coordinated NGs.<sup>[20]</sup> This result demonstrates that the Cu(II)@NGs-LA possess the potential application for MR imaging. Overall, these results confirm that according to the personalized needs, the availability of amino-terminal NGs for post-modification with different functional molecules renders advanced functional architectures for the potential applications of specific targeting, imaging, and theranostics of tumors.

#### 2.4. Photothermal Property under NIR I and II Windows

The formed Cu(II)@NGs-LA were further reacted with Na<sub>2</sub>S to in situ generate CuS@NGs-LA (Figure 4a). The CuS@NGs-LA aqueous solution showed dark green at a low concentration of 0.5 mg mL<sup>-1</sup> (Figure 4b). As expected, the CuS NPs (about 5–10 nm) are successfully loaded in the shell of NGs (Figure 4c), due to the Cu(II) binding on the periphery of NGs. The final Cu content within CuS@NGs-LA was detected by ICP-OES to be 57 μg mg<sup>-1</sup>. Remarkably, the CuS@NGs-LA

show uncommon structure of CuS loading compared to some previous literatures,<sup>[10b,21]</sup> where the CuS NPs are randomly distributed throughout NGs. Therefore, a novel structure regarding CuS NPs loaded in the shell of NGs was constructed. Moreover, UV-vis-NIR spectra evidenced that CuS@NGs-LA having an obvious absorption in the range of NIR I and II windows (700–1300 nm) render them with photothermal performance under NIR irradiation.

Notably, compared to the NIR I laser, the NIR II laser displays two significant advantages of higher maximum permissible exposure (MPE) and better tissue penetration depth.<sup>[22]</sup> According to the standard reported by the American National Standards Institute,<sup>[23]</sup> the MPE value for skin exposure of NIR II laser (1050–1400 nm) is 1.0 W cm<sup>-2</sup>, while that of NIR I laser (800–950 nm) is less than 0.6 W cm<sup>-2</sup>. In some recent work,<sup>[21,24]</sup> the photothermal property of CuS NPs loaded platforms under NIR I irradiation was investigated, and they were employed in vivo with a high power density (1–2 W cm<sup>-2</sup>) which exceeds the safe MPE value, to obtain excellent PTT of tumors. Moreover, the NIR II laser, especially in the range of 1000–1100 nm, is expected to achieve the maximal penetration depth.

Next, we not only explored the photothermal property of CuS@NGs-LA, but not compared their heating rate, PCE, and photothermal effect of deep tissue under 808 nm (NIR I) and 1064 nm (NIR II). After 1064 nm laser (0.6 W cm<sup>-2</sup>) irradiation for 300 s (Figure 4e), the temperature of water and NGs-LA did not emerge obvious change (less than 5 °C). For comparison, the temperature increasing of CuS@NGs-LA was rapid, and the increasing tendency was augment with sample



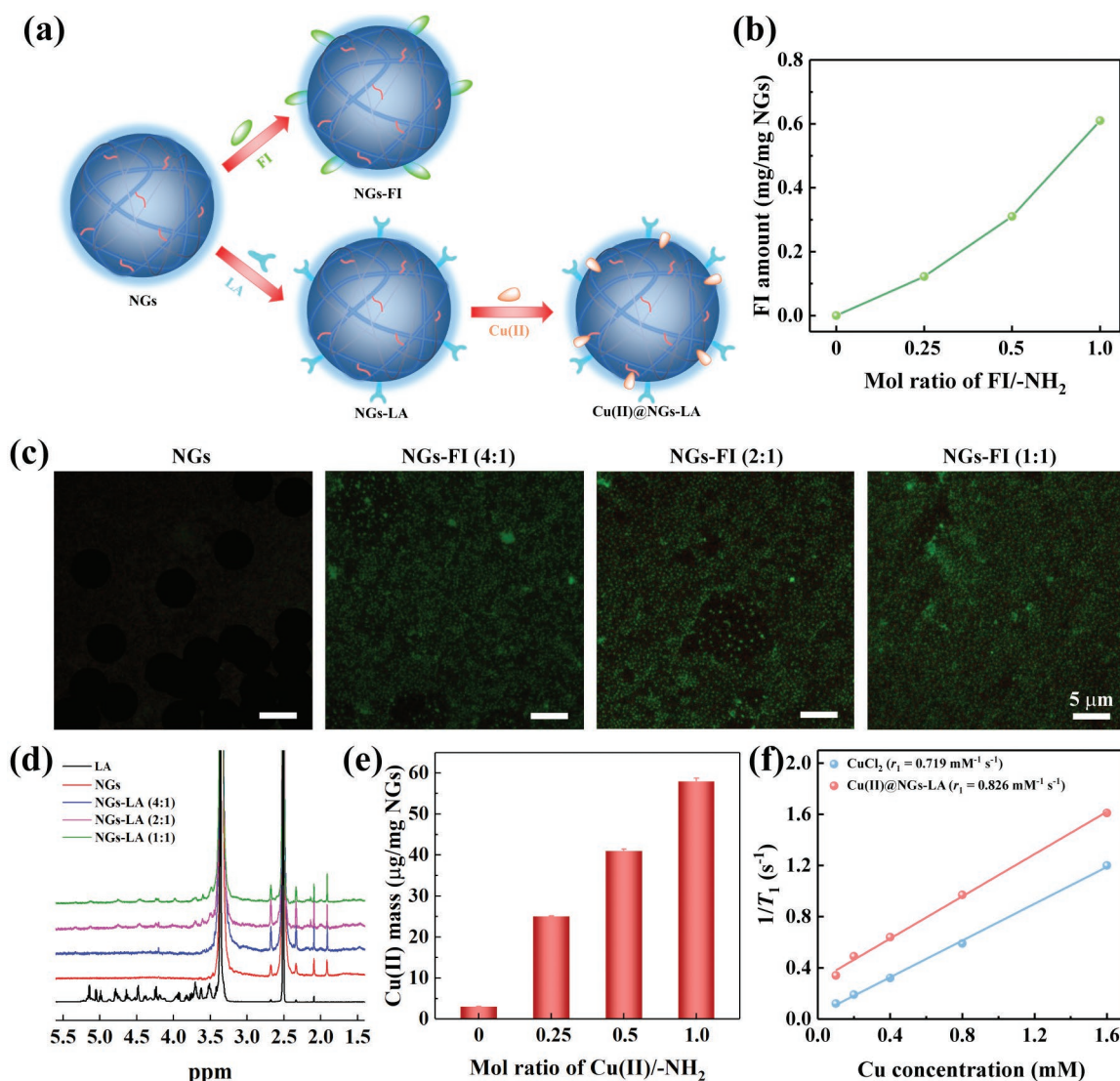


**Figure 3.** a) Schematic illustration of the multifunctional modification of NGs. b) The FI amounts and c) the fluorescence microscopic images of NGs-FI with different molar ratios of FI/-NH<sub>2</sub>. d) <sup>1</sup>H NMR spectra of LA, NGs and NGs-LA with different molar ratios of LA/-NH<sub>2</sub>. e) The Cu(II) loading amounts of Cu(II)@NGs-LA with different molar ratios of Cu(II)/-NH<sub>2</sub>. f) T<sub>1</sub> relaxation rate of Cu(II)@NGs-LA as a function of Cu(II) concentration.

concentrations. What is more, the temperature change ( $\Delta T$ ) of CuS@NGs-LA with different concentrations (1–3 mg mL<sup>-1</sup>) was quantified from 25.3 to 39.9 °C (Figure 4f). Next, the temperature increasing rates of CuS@NGs-LA upon 1064 nm (0.6 W cm<sup>-2</sup>) and 808 nm laser (0.6 and 1.2 W cm<sup>-2</sup>) were compared (Figure 4g). The  $\Delta T$  of CuS@NGs-LA solution (1 mg mL<sup>-1</sup>) was increased by 31.6 °C after 1064 nm laser irradiation for 300 s, while the  $\Delta T$  only increases by 11.4 °C after 808 nm laser (0.6 W cm<sup>-2</sup>) irradiation, even the laser power density doubled (1.2 W cm<sup>-2</sup>), it increased by 27.1 °C. Furthermore, the visualized photothermal images of water, NGs-LA, and CuS@NGs-LA aqueous solutions were captured (Figure 4i). These results demonstrate that CuS@NGs-LA upon 1064 nm laser with safe irradiation display better photothermal effect than that upon 808 nm laser with super-high power (beyond safe MPE value), since CuS@NGs-LA present stronger absorbance in NIR II window and the NIR II laser exhibit higher

MPE. Additionally, the PCE ( $\eta$ ) of CuS@NGs-LA exposed to 1064 nm (0.6 W cm<sup>-2</sup>) and 808 nm laser (0.6 and 1.2 W cm<sup>-2</sup>) was calculated to be 31.1%, 27.4%, and 28.6%, respectively (Figure 4h). Notably, the  $\eta$  of 31.1% is higher compared to the PCE of other CuS randomly loaded NGs reported in our previous work.<sup>[10b]</sup> This may be due to that the unique structure of CuS NPs loaded in the NGs shell permits to facilitate more full contact with NIR II laser, leading to the absorption and conversion of more laser into heat energy.

Apart from the aforementioned higher MPE of NIR II laser, the other most important advantage is its superior tissue penetration depth when compared to NIR I laser (Figure 5a). The photothermal effect of CuS@NGs-LA covered by chicken breast tissue with different depths under 808 and 1064 nm laser irradiation with same power was explored (Figure 5b). With the tissue thickness increasing, the  $\Delta T$  exhibited a decreasing trend upon both lasers. Remarkably, at same tissue

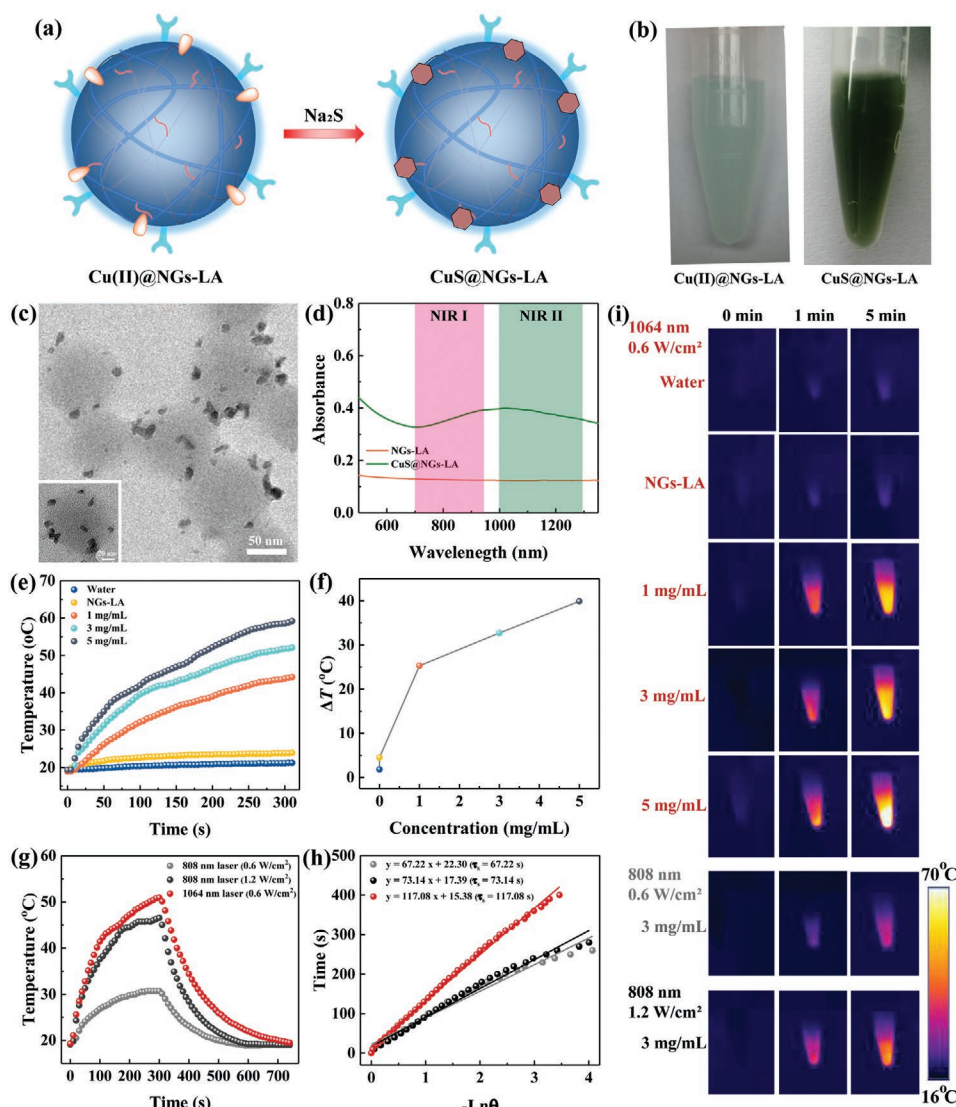


**Figure 4.** a) Schematic illustration of the preparation of CuS@NGs-LA. b) Digital photograph and c) TEM imaging of CuS@NGs-LA. d) UV-vis-NIR spectra of NGs-LA and CuS@NGs-LA. e) Temperature change of water, NGs-LA, and CuS@NGs-LA aqueous solution with different concentrations upon 1064 nm laser ( $0.6 \text{ W cm}^{-2}$ ) as function of time. f) Plot of temperature change ( $\Delta T$ ) over a period of 300 s versus the concentration of water, NGs-LA and CuS@NGs-LA. g) Photothermal effect of CuS@NGs-LA upon 1064 nm laser ( $0.6 \text{ W cm}^{-2}$ ) and 808 nm laser ( $0.6$  and  $1.2 \text{ W cm}^{-2}$ ). The laser was turned off after irradiation for 300 s. h) Plot of cooling time versus negative natural logarithm of the driving force temperature in the cooling stage. i) Thermal images of water, NGs-LA, and CuS@NGs-LA aqueous solution with different concentrations under irradiation of 1064 nm laser and 808 nm laser.

thickness, the  $\Delta T$  values upon 1064 nm laser were higher than that upon 808 nm laser. Even in relatively deep tissue (10 cm), the  $\Delta T$  can increase by  $7.3^\circ\text{C}$  which will cause an irreversible damage and significant necrosis for cancer cells *in vivo*.<sup>[25]</sup> This result indicates that CuS@NGs-LA possess enormous potentials for PTT of cancers upon 1064 nm laser with a safe irradiation.

## 2.5. Biocompatibility and Cellular Uptake

It is necessary to evaluate the biocompatibility of CuS@NGs-LA before their biomedical applications *in vivo*. By CCK-8 assay

(Figure S6, Supporting Information), the viability of HepG2 cells treated with CuS@NGs-LA only had slight decreases and remained above 87.1% at a maximum concentration of  $500 \mu\text{g mL}^{-1}$ , indicating CuS@NGs-LA emerge excellent biocompatibility. Moreover, the LA-mediated targeting specificity of CuS@NGs-LA for HepG2 cells was checked by Cu element uptake using quantitative ICP-OES analysis (Figure S7, Supporting Information). Clearly, the Cu uptake exhibited a concentration-dependent increasing in both HepG2-HR and HepG2-LR cells. At the same concentration, the Cu uptake in HepG2-HR cells was significantly higher (around 1.9–2.4 times) than that in HepG2-LR cells, revealing that the modification of LA renders the CuS@NGs-LA with targeting specificity to HepG2-HR cells.

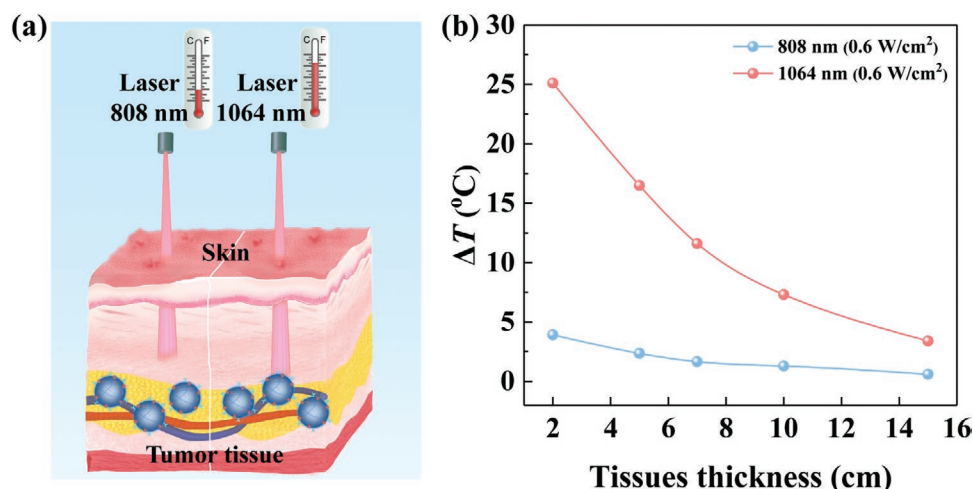


**Figure 5.** a) Schematic illustration of the photothermal effect of CuS@NGs-LA at deep-tissue upon 808 or 1064 nm laser. b) Temperature decay of CuS@NGs-LA at different depths of chicken breast tissue upon 808 or 1064 nm laser.

## 2.6. pH/NIR/Redox Multi-Triggered Drug Release

The CuS@NGs-LA were employed as nanocarriers to encapsulate drug (DOX), which was characterized via UV-vis spectra and fluorescence microscopic imaging. Compared to CuS@NGs-LA, an apparent absorption peak of CuS@NGs-LA/DOX at 480 nm was observed, and this feature peak was associated to the entrapped DOX (Figure 6a). Likewise, the CuS@NGs-LA/DOX displayed the red fluorescence from DOX (Figure 6b,c), and the DOX loading efficiency of CuS@NGs-LA/DOX was further calculated to be 78.4%. For an ideal drug release, it is indispensable to achieve controllable release capability, including switching on and off drug supply, to maintain the effective drug concentration at the required time in vivo for realizing a continuous therapeutic effect.<sup>[26]</sup> Next, the controlled DOX release behaviors of CuS@NGs-LA/DOX were determined under pH 7.4, pH 6.5, pH 5.5, pH 5.5 with NIR, and pH 5.5 with GSH (Figure 6d). The DOX released quickly and the cumulative release amount reached 44.1% and 32.1% under pH 5.5 and pH 6.5 after 24 h, respectively, which is higher than that under pH 7.4 (8.7%), due to the proton sponge effect. It is noteworthy that, after 1064 nm laser irradiation for 10 min intervals, the DOX release dramatically increased,

and the final cumulative amount was 59.2%. The controllable on/off release based on NIR irradiation should be attributed to the shrinking/swelling of NGs which is caused by the controllable temperature change (above or below the VPTT of NGs). Moreover, under GSH condition, the DOX release rate was high, and  $\approx 79.2\%$  of DOX was released owing to the degradation of NGs. Taking together, CuS@NGs-LA/DOX could be introduced as a promising drug-loaded nanocarrier with multi-triggered controlled drug release, involving endogenous of TME (pH/GSH) and exogenous of NIR laser, for improving anticancer activity and reducing side effects. In comparison with conventional single factor-triggered nanocarriers, the developed nanoplateforms are able to control drug release efficiently by responding to endogenous factors and regulating exogenous stimuli simultaneously, revealing an innovative and smart release mode.

## 2.7. Combinational Photothermal Therapy and Chemotherapy In Vitro

Among the existing cancer therapy strategies, the combination of efficient PTT and controllable CMT may be a promising

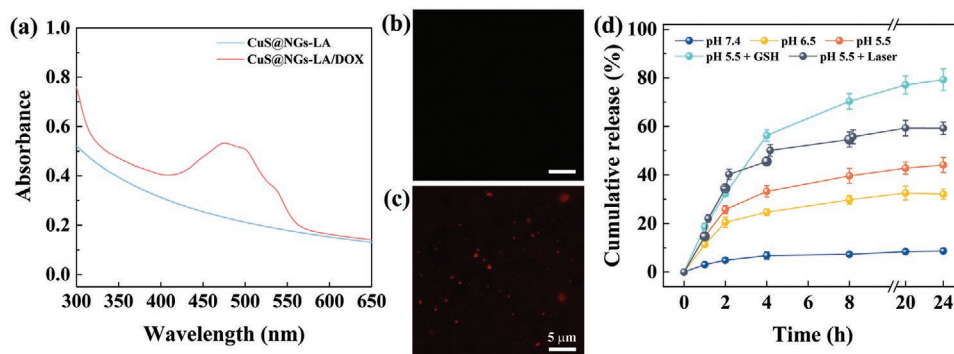


**Figure 6.** a) UV-vis spectra of CuS@NGs-LA and CuS@NGs-LA/DOX. Fluorescence microscopic images of b) CuS@NGs-LA and c) CuS@NGs-LA/DOX. d) Time-dependent DOX cumulative release from CuS@NGs-LA/DOX under pH 7.4, pH 6.5, pH 5.5, pH 5.5 with NIR laser (1064 nm, 0.6 W cm<sup>-2</sup>, 10 min), and pH 5.5 with GSH (10 mM). In pH 5.5 + Laser group, large and small ball represent laser on and off, respectively.



method to achieve compelling tumor elimination and recurrence suppression, due to their distinct advantages. The anti-cancer efficacy of CuS@NGs-LA/DOX upon 1064 nm laser with safe irradiation ( $0.6 \text{ W cm}^{-2}$ ) was verified (Figure 7a).

The viability of HepG2 cells in control groups maintained at a relatively high level in the studied concentrations, while the significant decreasing of cell viability in CuS@NGs-LA + Laser, CuS@NGs-LA/DOX and CuS@NGs-LA/DOX + Laser groups

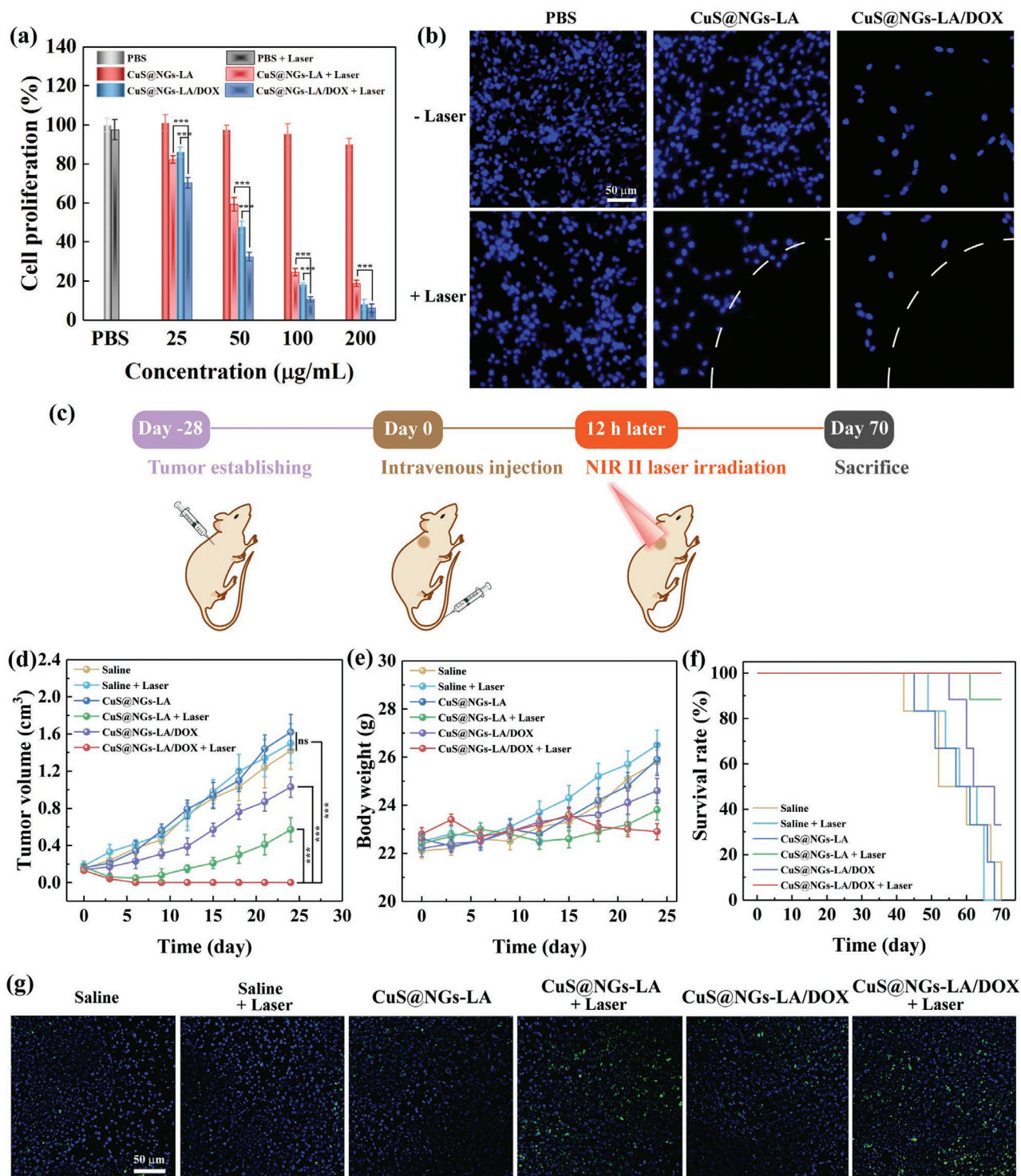


**Figure 7.** a) CCK-8 assay of HepG2 cells in different groups. b) Fluorescence microscopic images of cells with nuclei stained by DAPI (blue) in different groups. Blue fluorescence is the living cell nuclei stained with DAPI and dark regions represent the dead cells exfoliated from cell walls. c) Schematic illustration of the administration process used for the combined therapy of advanced tumors in vivo. d) Tumor volume, e) body weight, and f) survival rate of mice bearing HepG2 xenografted tumors in different groups for different periods. g) TUNEL staining of tumor sections in different groups.

was observed with the concentration increase. Notably, the cells in CuS@NGs-LA/DOX + Laser group (combined therapy) displayed lower viability when compared to that in CuS@NGs-LA + Laser group (single PTT) or CuS@NGs-LA/DOX group (single CMT). These results reveal that the combinational PTT and CMT can indeed achieve enhanced anticancer effect compared with the PTT and CMT alone.

Furthermore, through the visualization of fluorescence microscopic imaging after cell staining (Figure 7b), the HepG2 cells in CuS@NGs-LA + Laser, CuS@NGs-LA/DOX, and CuS@NGs-LA/DOX + Laser groups showed scarce living and large dead, and only the smallest amount of cells was alive in CuS@NGs-LA/DOX + Laser group. While the cells in control groups emerged regular cell shapes, and large number of living cells was observed in the entire region of cell walls. These results once again demonstrate that the developed CuS@NGs-LA/DOX under NIR II laser with safe irradiation is able to enhance anticancer efficacy by the combined therapy.

## 2.8. Combination Therapy of Advanced Tumors In Vivo

To prove the effective PTT of CuS@NGs-LA/DOX in vivo upon safe NIR II irradiation, the thermal images and temperature changes of tumor were collected using thermal imaging system (Figure S8, Supporting Information). Compared to PBS group, the temperature of tumor in CuS@NGs-LA/DOX group displayed obvious increasing from about 38.8–51.9 °C. According to the previous work,<sup>[10b,25a]</sup> tumor cells can be ablated irreversibly at the temperature of more than 45 °C.

In some precious reported work,<sup>[27]</sup> the evaluation of cancer treatment effect is mainly based on the early tumors with a small volume of 0.05–0.07 cm<sup>3</sup>. To investigate the excellent antitumor efficacy of combined PTT and CMT using CuS@NGs-LA/DOX under safe NIR II irradiation in vivo, we constructed the tumor model in mice with large volume (0.15–0.20 cm<sup>3</sup>) to simulate the advanced tumors (Figure 7c,d). Apparently, the tumors in control groups emerged significant growth with the time post-injection. In our previous results,<sup>[27a,b]</sup> the early tumors can be ablated completely after single PTT. However, the advanced tumors were only inhibited to some extent in CuS@NGs-LA + Laser and CuS@NGs-LA/DOX groups, suggesting that these advanced tumors cannot be eradicated by single treatment, even with highly effective PTT upon NIR II laser. Encouragingly, in CuS@NGs-LA/DOX + Laser group, the advanced tumors were eliminated thoroughly on day 6 post-treatment and the tumors did not reoccur afterward. Additionally, the survival rates of mice in different groups were monitored to further explore the antitumor efficacy of the combined therapy (Figure 7f). On the day 65–70 after treatment, the mice in control groups were all dead, while the mice in CuS@NGs-LA/DOX + Laser group exhibited a 100% survival rate which was higher than that in CuS@NGs-LA + Laser (88.3%) and CuS@NGs-LA/DOX groups (33.2%). By TUNEL staining of tumor sections, large part of necrosis was observed in CuS@NGs-LA + Laser, CuS@NGs-LA/DOX and CuS@NGs-LA/DOX + Laser groups (Figure 7g). Furthermore, the cell apoptosis rates were analyzed quantitatively (Figure S9, Supporting Information), and follows the order of CuS@NGs-LA/DOX + Laser group (56.8%)

> CuS@NGs-LA + Laser group (41.3%) > CuS@NGs-LA/DOX group (12.7%) > Control groups (4.1–6.2%). These results imply that the combined therapy exerts higher potency in advanced tumors treatment and prolonger survival life-span than PTT and CMT alone. This should be attributed to these owned advantages of LA-mediated targeting, efficient PTT upon NIR II laser, promoted drug release induced by acidic TME and NIR II laser as well as redox-triggered degradation of CuS@NGs-LA/DOX.

Moreover, the negligible systemic toxicity for mice after treatment is necessary. All of mice in different groups did not show obvious weight loss during 24 days (Figure 7e). To further evaluate the long-term side effects, the main organs (i.e., heart, liver, spleen, lung, and kidney) of mice in different groups were removed and H&E stained on day 24 (Figure S10, Supporting Information). Clearly, no any necrosis region of these organs was observed. These results suggest that the designed nano-platforms and strategy not only obtain superior tumor elimination and recurrence suppression for advanced tumors but also exhibit negligible adverse effects in vivo.

Finally, after intravenous injection of CuS@NGs-LA/DOX, the in vivo biodistribution of Cu element was determined by ICP-OES (Figure S11, Supporting Information). The accumulated amount of Cu element in the tumor reached the highest level at 12 h post-injection, and the relatively high level was maintained until 48 h, due to LA-mediated specific targeting. Likewise, the Cu element was metabolized from the liver and spleen, suggesting that the NGs after administration can be cleared by the reticuloendothelial system organs.

## 3. Conclusion

In summary, using the novel strategy of modular molecular engineering, the versatile theranostic nano-platforms based on cationic NGs were designed for highly efficient treatment of tumors. The cationic NGs with uniform morphology, pH/thermal dual-responsive behaviors and redox-triggered degradation were first synthesized using facile one-step synthesis. According to the individual requirement, the NGs would be further functionalized to achieve fluorescent property,  $r_1$  relaxivity, strong absorption in NIR I and II windows, high PCE, excellent biocompatibility, and specific targeting ability in a modular manner. The novel hybrid CuS@NGs-LA were obtained by loading of CuS NPs in the shell of NGs, that possess higher PCE than the CuS randomly loaded NGs reported in previous work. Moreover, the superior photothermal effect in NIR II over NIR I window is presented due to higher PCE and deeper tissue penetration. Remarkably, the CuS@NGs-LA/DOX display excellent photothermal effect upon 1064 nm laser with safe irradiation, and controlled drug release in responding to multi-stimulus (endogenous pH/redox and exogenous NIR), which can be employed to completely eliminate advanced solid tumors and effectively inhibit recurrence by the combined PTT and CMT. The developed pervasive nano-platforms based on cationic NGs with tunable responsiveness, versatility, and biodegradation by novel strategy is able to address some current challenges, and the intelligent nano-platforms serve as useful tool for the next generation of personalized theranostic protocol.

## 4. Experimental Section

**Synthesis of Core/Shell Structured PVCL-NH<sub>2</sub> Nanogels:** The amino-terminal PVCL-based NGs with core/shell structure were synthesized using precipitation polymerization approach. The VCL (1.92 g, 13.8 mmol), DADS (43.9 mg, 0.3 mmol), and CTAB (20.7 mg) were dissolved in water (144 mL), and then purged with nitrogen in a double wall reactor under stirring at 70 °C for 30 min to achieve a complete homogenization. AMPA (55.0 mg, 0.2 mmol), and VFA (50.4 mg, 1.2 mmol) were dissolved in water (1 mL), respectively, and then purged with nitrogen for 30 min. Subsequently, the AMPA acting as a free-radical initiator was added into the mixture with the speed of 1.0–1.2 mL h<sup>-1</sup> using a pump to ensure the location of VFA in the shell of the NGs. After that, the polymerization was carried out for additional 2–3 h, and then NaOH (500 mg, 12.5 mmol) was added to the above solution and stirred at 70 °C for 48 h. The reaction mixture was taken out separately from the reactor before and after NaOH adding for different times (0–48 h). Finally, the dispersions were dialyzed against water using dialysis membrane (MWCO = 8000–14 000) for 3 days, and freeze-dried. The core/shell structured NGs before and after hydrolysis for 1 h were named as PVCL-VFA NGs and PVCL-NH<sub>2</sub> NGs 1h, respectively, and other NGs were named in a similar manner.

**Multifunctional Modification:** The fluorescent molecules FI were labeled on the NGs to form NGs-FI by the isothiocyanate-amine coupling reaction. Briefly, the FI with different contents (molar ratios of FI/-NH<sub>2</sub> from 1:4 to 1:1, in DMSO) were mixed with the NGs dissolved in DMSO (5 mg mL<sup>-1</sup>, 1 mL), respectively, and then stirred at room temperature overnight. Afterward, the mixtures were dialyzed against water using dialysis membrane (MWCO = 8000–14 000) for 3 days and freeze-dried to obtain FI-labeled NGs which with different molar ratios of -NH<sub>2</sub>/FI were named as NGs-FI (4:1), NGs-FI (2:1), and NGs-FI (1:1).

Moreover, the targeted molecule LA was conjugated on the NGs to prepared NGs-LA via EDC chemistry. The LA with different contents (molar ratios of LA/-NH<sub>2</sub> from 1:4 to 1:1, in DMSO) were activated by 5 equivalent of EDC (in DMSO) under stirring for 30 min, and then 5 equivalent of NHS (in DMSO) was added for another 3 h. After that, the NGs dissolved in DMSO (5 mg mL<sup>-1</sup>, in 1 mL) was added to the above solution respectively under stirring for 3 days. The mixtures were dialyzed and freeze-dried to achieve LA-conjugated NGs according to the aforementioned protocol, and these formed NGs with different molar ratios of LA/-NH<sub>2</sub> were named as NGs-LA (4:1), NGs-LA (2:1), and NGs-LA (1:1).

Next, to reserve part of the amino groups for further modification, the prepared NGs-LA (2:1) were employed to bind Cu(II) through the carbonyl and amino groups of NGs-LA. In brief, the CuCl<sub>2</sub>·2H<sub>2</sub>O with different contents (molar ratios of Cu(II)/-NH<sub>2</sub> from 1:4 to 1:1, in water) were reacted with the NGs-LA dissolved in water (5 mg mL<sup>-1</sup>, 1 mL), respectively, under stirring for 24 h. Subsequently, these mixtures were centrifuged (8000 rpm, 20 min) to get Cu(II)@NGs-LA.

**Synthesis of CuS@NGs-LA:** The prepared Cu(II)@NGs-LA under the molar ratio of 1:1 were used as templates to form CuS@NGs-LA in situ. The Cu(II)@NGs-LA (20 mg, in 10 mL water) were mixed with Na<sub>2</sub>S·9H<sub>2</sub>O solution (15 mg, in 1 mL water) under stirring at 35 °C overnight. Finally, the mixture was dialyzed and freeze-dried to obtain CuS@NGs-LA according to the aforementioned protocol.

**Characterization of Functionalized Nanogels:** The pH/thermal/redox multi-responsive behavior, fluorescence property,  $\tau_1$  relaxivity, photothermal property under NIR I/II windows, and pH/redox/NIR multi-responsive controlled drug release of the functionalized NGs.

**In Vitro Cell Culture and Assays:** HepG2 cells (a human liver cancer cell line) were regularly cultured and passaged for cytocompatibility, targeting specificity, and anticancer activity assays of the functionalized NGs.

**In Vivo Animal Experiments:** All animal experiments were approved by the Ethical Committee of Shanghai Zhongshan Hospital and also followed the policy of the National Ministry of Health (B2019-136R2). The functionalized NGs were subjected to tumor accumulation and combined anticancer efficacy assays in vivo. See additional details in Supporting Information.

## Supporting Information

Supporting Information is available from the Wiley Online Library or from the author.

## Acknowledgements

X.L. and H.S. contributed equally to this work. This research was financially supported by the Sino-German Center for Research Promotion (GZ1505), Deutsche Forschungsgemeinschaft (SFB 985, Functional Microgels and Microgel Systems), National Natural Science Foundation of China (81761148028), Science and Technology Commission of Shanghai Municipality (19XD1400100), and China Scholarship Council (for X.L.). The authors would like to especial thank Silke Reider for STEM images.

Open access funding enabled and organized by Projekt DEAL.

## Conflict of Interest

The authors declare no conflict of interest.

## Data Availability Statement

Research data are not shared.

## Keywords

cationic nanogels, modular engineering, multi-responsiveness, theranostics

Received: January 8, 2021

Revised: February 6, 2021

Published online:

- [1] a) J. J. Green, J. H. Elisseeff, *Nature* **2016**, *540*, 386; b) J. D. Martin, H. Cabral, T. Stylianopoulos, R. K. Jain, *Nat. Rev. Clin. Oncol.* **2020**, *17*, 251; c) E. K. H. Chow, D. Ho, *Sci. Transl. Med.* **2013**, *5*, 216rv4.
- [2] a) J. R. Clegg, A. S. Irani, E. W. Ander, C. M. Ludolph, A. K. Venkataraman, J. X. Zhong, N. A. Peppas, *Sci. Adv.* **2019**, *5*, eaax7946; b) K. M. Koo, P. N. Mainwaring, S. A. Tomlins, M. Trau, *Nat. Rev. Urol.* **2019**, *16*, 302.
- [3] a) F. Seidi, R. Jenjob, D. Crespy, *Chem. Rev.* **2018**, *118*, 3965; b) O. Adir, M. Poley, G. Chen, S. Froim, N. Krinsky, J. Shklover, J. Shainsky-Roitman, T. Lammers, A. Schroeder, *Adv. Mater.* **2020**, *32*, 1901989; c) P. Koczera, L. Appold, Y. Shi, M. J. Liu, A. Dasgupta, V. Pathak, T. Ojha, S. Fokong, Z. J. Wu, M. van Zandvoort, O. Iranzo, A. J. C. Kuehne, A. Pich, F. Kiessling, T. Lammers, *J. Controlled Release* **2017**, *259*, 128.
- [4] a) S. Y. Lu, X. Li, J. L. Zhang, C. Peng, M. W. Shen, X. Y. Shi, *Adv. Sci.* **2018**, *5*, 1801612; b) X. Li, L. X. Xing, Y. Hu, Z. J. Xiong, R. Z. Wang, X. Y. Xu, L. F. Du, M. W. Shen, X. Y. Shi, *Acta Biomater.* **2017**, *62*, 273.
- [5] a) S. Q. He, J. Song, J. L. Qu, Z. Cheng, *Chem. Soc. Rev.* **2018**, *47*, 4258; b) J. Yang, R. Xie, L. L. Feng, B. Liu, R. C. Lv, C. X. Li, S. L. Gai, F. He, P. P. Yang, J. Lin, *ACS Nano* **2019**, *13*, 13144.
- [6] L. X. Xing, X. Li, Z. H. Xing, F. Li, M. W. Shen, H. Wang, X. Y. Shi, L. F. Du, *Chem. Eng. J.* **2020**, *382*, 122949.
- [7] a) X. S. Li, J. F. Lovell, J. Yoon, X. Y. Chen, *Nat. Rev. Clin. Oncol.* **2020**, *17*, 657; b) M. Dunne, M. Regenold, C. Allen, *Adv. Drug Delivery Rev.* **2020**, *163–164*, 98.
- [8] a) X. Li, S. Y. Lu, Z. G. Xiong, Y. Hu, D. Ma, W. Q. Lou, C. Peng, M. W. Shen, X. Y. Shi, *Adv. Sci.* **2019**, *6*, 1901800; b) Z. C. Xiao, Z. W. Su, S. S. Han, J. S. Huang, L. T. Lin, X. T. Shaoi, *Sci. Adv.*



- 2020, 6, eaay7785; c) X. Li, Z. G. Xiong, X. Y. Xu, Y. Luo, C. Peng, M. W. Shen, X. Y. Shi, *ACS Appl. Mater. Interfaces* **2016**, 8, 19883.
- [9] a) Y. L. Li, D. Maciel, J. Rodrigues, X. Y. Shi, H. Tomas, *Chem. Rev.* **2015**, 115, 8564; b) A. Scotti, S. Bochenek, M. Brugnoli, M. A. Fernandez-Rodriguez, M. F. Schulte, J. E. Houston, A. P. H. Gelissen, I. I. Potemkin, L. Isa, W. Richtering, *Nat. Commun.* **2019**, 10, 1418; c) R. Keidel, A. Ghavami, D. M. Lugo, G. Lotze, O. Virtanen, P. Beumers, J. S. Pedersen, A. Bardow, R. G. Winkler, W. Richtering, *Sci. Adv.* **2018**, 4, eaao7086.
- [10] a) F. A. Plamper, W. Richtering, *Acc. Chem. Res.* **2017**, 50, 131; b) C. C. Zhang, W. J. Sun, Y. Wang, F. Xu, J. Qu, J. D. Xia, M. W. Shen, X. Y. Shi, *ACS Appl. Mater. Interfaces* **2020**, 12, 9107; c) H. Peng, W. J. Xu, A. Pich, *Polym. Chem.* **2016**, 7, 5011.
- [11] a) A. L. Wu, Y. X. Guo, X. B. Li, H. M. Xue, J. B. Fei, J. B. Li, *Angew. Chem., Int. Ed.* **2021**, 60, 2099; b) M. J. Xuan, J. X. Shao, J. B. Li, *Natl. Sci. Rev.* **2019**, 6, 551; c) Y. Cui, J. B. Fei, J. B. Li, *Sci. Sin.: Chim.* **2011**, 41, 273.
- [12] C. Song, M. W. Shen, J. Rodrigues, S. Mignani, J. P. Majoral, X. Y. Shi, *Coord. Chem. Rev.* **2020**, 421, 213463.
- [13] F. Abedi-Gaballu, G. Dehghan, M. Ghaffari, R. Yekta, S. Abbaspour-Ravasjani, B. Baradaran, J. E. N. Dolatabadi, M. R. Hamblin, *Appl. Mater. Today* **2018**, 12, 177.
- [14] S. Sindhwani, A. M. Syed, J. Ngai, B. R. Kingston, L. Maiorino, J. Rothschild, P. MacMillan, Y. W. Zhang, N. U. Rajesh, T. Hoang, J. L. Y. Wu, S. Wilhelm, A. Zilman, S. Gadde, A. Sulaiman, B. Ouyang, Z. Lin, L. S. Wang, M. Egeblad, W. C. W. Chan, *Nat. Mater.* **2020**, 19, 566.
- [15] Q. Zhou, S. Q. Shao, J. Q. Wang, C. H. Xu, J. J. Xiang, Y. Piao, Z. X. Zhou, Q. S. Yu, J. B. Tang, X. R. Liu, Z. H. Gan, R. Mo, Z. Gu, Y. Q. Shen, *Nat. Nanotechnol.* **2019**, 14, 799.
- [16] E. Gau, F. Flecken, T. Belthle, M. Ambarwati, K. Loos, A. Pich, *Macromol. Rapid Commun.* **2019**, 40, 1900144.
- [17] H. Peng, X. B. Huang, A. Melle, M. Karperien, A. Pich, *J. Colloid Interface Sci.* **2019**, 540, 612.
- [18] a) R. A. Meurer, S. Kemper, S. Knopp, T. Eichert, F. Jakob, H. E. Goldbach, U. Schwaneberg, A. Pich, *Angew. Chem., Int. Ed.* **2017**, 56, 7380; b) T. Wen, F. Qu, N. B. Li, H. Q. Luo, *Arabian J. Chem.* **2017**, 10, S1680; c) Z. X. Wu, F. A. Fernandez-Lima, D. H. Russell, *J. Am. Soc. Mass Spectrom.* **2010**, 21, 522; d) Y. Fan, W. J. Sun, X. Y. Shi, *Small Methods* **2017**, 1, 1700224.
- [19] a) Y. Fan, L. Z. Lin, F. F. Yin, Y. Zhu, M. W. Shen, H. Wang, L. F. Du, S. Mignani, J. P. Majoral, X. Y. Shi, *Nano Today* **2020**, 33, 100899; b) Y. Fan, J. L. Zhang, M. H. Shi, D. Li, C. H. Lu, X. Y. Cao, C. Peng, S. Mignani, J. P. Majoral, X. Y. Shi, *Nano Lett.* **2019**, 19, 1216.
- [20] W. J. Sun, S. Thies, J. L. Zhang, C. Peng, G. Y. Tang, M. W. Shen, A. Pich, X. Y. Shi, *ACS Appl. Mater. Interfaces* **2017**, 9, 3411.
- [21] T. Shu, Q. M. Shen, L. Su, X. J. Zhang, M. J. Serpe, *ACS Appl. Nano Mater.* **2018**, 1, 1776.
- [22] a) J. C. Li, K. Y. Pu, *Acc. Chem. Res.* **2020**, 53, 752; b) F. Ding, Y. B. Zhan, X. J. Lu, Y. Sun, *Chem. Sci.* **2018**, 9, 4370; c) J. Li, Y. Liu, Y. L. Xu, L. Li, Y. Sun, W. Huang, *Coord. Chem. Rev.* **2020**, 415, 213318.
- [23] ANSI, **2000**, Laser Institute of America: Orlando.
- [24] M. Y. Zhang, X. J. Liu, Q. Luo, Q. Wang, L. J. Zhao, G. Y. Deng, R. B. Ge, L. Zhang, J. Q. Hu, J. Lu, *Chem. Eng. J.* **2020**, 389, 124450.
- [25] a) E. M. Knavel, C. L. Brace, *Tech. Vasc. Interventional Radiol.* **2013**, 16, 192; b) J. R. Wu, D. H. Bremner, S. W. Niu, M. H. Shi, H. J. Wang, R. R. Tang, L. M. Zhu, *ACS Appl. Mater. Interfaces* **2018**, 10, 42115.
- [26] Z. Shi, J. Wu, Q. Song, R. Göstl, A. Herrmann, *J. Am. Chem. Soc.* **2020**, 142, 14725.
- [27] a) C. Cai, X. Li, Y. Wang, M. X. Liu, X. Y. Shi, J. D. Xia, M. W. Shen, *Chem. Eng. J.* **2019**, 362, 842; b) X. Li, L. X. Xing, K. L. Zheng, P. Wei, L. F. Du, M. W. Shen, X. Y. Shi, *ACS Appl. Mater. Interfaces* **2017**, 9, 5817; c) H. P. Lee, A. K. Gaharwar, *Adv. Sci.* **2020**, 7, 2000863.